Journal of Mathematical Chemistry, Vol. 42, No. 4, November 2007 (© 2006)
DOI: 10.1007/s10910-006-9146-1

Model hysteresis dimer molecule I: Equilibrium properties

Christopher G. Jesudason*

Chemistry Department, University of Malaya, pantai valley, 50603 Kuala Lumpur, Peninsula, Malaysia
E-mail: Jesu@um.edu.my

Received 23 March 2006; revised 17 April 2006

A Hamiltonian system describing hysteresis behavior in a dimeric chemical reaction is modeled in a MD simulation utilizing novel two-body potentials with switches that is particularly suitable for numerical thermodynamical investigations. It is surmized that such reaction mechanisms could exist in nature on the basis of recent experiments, which indicate that electromagnetic hysteresis behavior is exhibited at the molecular level, although experimental interpretations tend to construct models that avoid such mechanisms. Numerical results of various common equilibrium thermodynamical and kinetic properties are presented together with new algorithms that were implemented to compute these quantities, where no unusual thermodynamics was observed for the chemical reaction which might be interpreted as not being "time reversible invariant" and therefore susceptible to manifesting unusual thermodynamical phenomena, which might contradict any of the known laws of thermodynamics. A revision of the concept of "time reversibility" to accommodate the above results is suggested. The general design of the reaction mechanism also allows for the use of conventional potentials and by the utilization of switches, overcomes the bottleneck of computations which involves multi-body interactions.

KEY WORDS: hysteresis chemical reaction model, thermodynamics of reaction, kinetic properties

2000 AMS mathematics classification: 65-{04,Z05}, 68-{04,W01} 70-{08,F01,F16}

1. Introduction

Recently, experiments have detected the presence of magnetic hysteresis behavior at the single molecule level [1, 2]; synthesis of such systems are also

*The initial theoretical, program and algorithm development was done at Norwegian University of Science and Technology-NTNU, Institute of Physical Chemistry, (Trondheim, Norway) during a sabbatical visit 2000–2001 financed by University of Malaya. The method of MD used here conforms to the periodic boundary conditions and thermostatting algorithms developed or refined by Ikeshoji and Hafskjold for standard, non-reacting particles. Their approach is non-synthetic using traditional Verlet integration of Newton's equations of motion.

a hot topic of research [3]. Such facts suggest that non-single-valued functions are involved in the phase trajectory of the system. A rational extension of this concept, which has profound theoretical implications is to construct a dynamical trajectory where the region of formation of the molecule does not coincide with that of its breakdown. There has been a reluctance in the past to consider such loop or hysteresis systems because of the absence of experimental evidence of hysteresis behavior at the molecular level, and because of the influence of the belief of "time-symmetry" invariance, which discourages such a view, which lead to the construction of dynamical pathways, which were both single valued and which did not have any loop or circular topology; a detailed mathematical examination of these common time symmetry presuppositions – so essential to physics – has been made [4,5] and it was shown that such views are often not warranted or incorrect. This work reports a workable model hysteresis reaction pathway, which leads to thermodynamically consistent behavior, exhibiting properties that will require new developments in reaction theory, and it also predicts the feasibility of such mechanisms in nature. It suggests a re-definition and extension of the ideas of "time reversibility" and "microscopic reversibility" to cater for the proposed mechanism. The dimeric particle reaction simulated may be written

$$2\mathrm{A} \underset{k_{-1}}{\overset{k_1}{\rightleftarrows}} \mathrm{A}_2, \tag{1}$$

where k_1 is the forwards rate constant and k_{-1} is the backwards rate constant. The reaction simulation was conducted at a mean temperature, which is very high, about $T^*_{\mathrm{set}} = T^* = 8.0$ well above the supercritical regime of the LJ fluid by a factor of 10 times the magnitude of normal simulation temperatures in reduced units. At these temperatures, the normal choices for time step increments do not obtain without also taking into account energy-momentum conservation algorithms in regions where there are abrupt changes of gradient. The total system temperature for this equilibrium simulation has an uncertainty of about 10^{-5} LJ units when all particles, whether atomic or dimeric are sampled; all other quantities determined have greater uncertainty, due to the smaller presence of the species, or if only a layer in the cell is sampled for runs of less than 5M time steps. There have been various attempts in modeling chemical reactions with different objectives in mind [6–11]. Some used generalized models with few details to predict the main features experiments might reveal [6] at the reaction coordinate close to the transition state (TS), such as what might occur within a solvent-caged reaction complex: $\mathrm{A–H}\cdots\mathrm{B} \rightleftharpoons \mathrm{A}\cdots\mathrm{H–B}$. This particular pioneering approach [6] was further elaborated by Bergsma et al. [11] in order to examine the limits of validity of TS theory (TST) by not carrying out an *ab initio* study of all the possible reactive trajectories, but by examining trajectories constrained to the TS surface because of the limits of computing power. An example of an

ab initio detailed chemical reaction approach with a 1,000 atom system using an assumed three body potential for the exchange process $F+F_2 \rightleftharpoons F_2+F$ is that of Ref. [9] who admit that the procedure was "very demanding". The current study involves 4,096 particles or atoms, and therefore is much improved where statistics are concerned. At the other extreme are generalized studies of hypothetical schemes [8] such as the "chemical reaction" $A+A \rightleftharpoons B+B$ used to elucidate some kinetic properties. Clearly, in such models, species A and B must represent complex systems that can be physically distinguished; in chemical applications, they might represent for instance *cis* and *trans* isomers of some compound or they might represent mesoscopic species. Some simulations do away altogether with the details of molecular dynamics based on dynamical laws [7], replacing them with the Ansatz that the details of the interaction between individual particles are not essential in the study of the statistical evolution of the system. Such an approach would make studies attempting to correlate the details of the dynamics to macroscopic properties difficult or obscure, despite the great savings in computer time, and therefore does not suite the purposes at hand here. The objectives of the present study include as follows:

(a) designing a mechanically well defined reaction model with low-computational demands and where the averaged motions of the dimer may be correlated with the macroscopic kinetic and thermodynamical properties and where no anomalies must be observed in the macroscopic results. Such an outcome would imply that the dynamics are reliable enough to be used in other studies.

(b) introducing some degree of complexity to the dimer such as vibrational and rotational states for more detailed dynamical investigations.

(c) utilizing the thermodynamically consistent model (as judged by the results of an equilibrium simulation) in nonequilibrium simulations.

Here we focus primarily on (a) above. To this end a new general algorithm (which will be discussed separately in another planned work) was used to conserve momentum and energy; (b) is represented in rotational studies and (c) in an NEMD simulation.

The following essential thermokinetic parameters will be determined and discussed in the sections that follows:

- The thermodynamic equilibrium constant through extrapolating the density to zero.
- The activity coefficient ratio.
- The standard Gibbs free energy, enthalpy and entropy of the reaction through extrapolation.

- The Arrhenius activation energy and pre-exponential terms, which bears no immediate connection to the potential of activation in figure 1, and the rate constants of the forward and reverse reactions.
- Self Diffusion and rotational diffusion constants.
- The probability distribution for the kinetic energy of a labeled atom to test the Gibbs ensemble postulate relative to the dynamic (switching) Hamiltonians used here. Within experimental error, there appears to be full conformity to the Gibbs thermodynamical postulates.

The method appears very promising for quantitative simulations of real systems, and will be utilized in the years ahead for various reaction studies, including those for conventional molecules.

2. The model

We examine the dimeric particle reaction given in (1) above

$$2\mathrm{A} \rightleftharpoons \mathrm{A}_2$$

in a range of equilibrium fluid states all well above the LJ supercritical regime. This model resembles somewhat that of Ref. [8] except that a harmonic potential is coupled to the products to form the bond of the dimer whenever the internuclear distance reaches the critical value r_f between two free atoms A.

In the current study, the potentials as given in figure 1 are used, but other configurations are possible, as verified by direct simulation, such as the excited

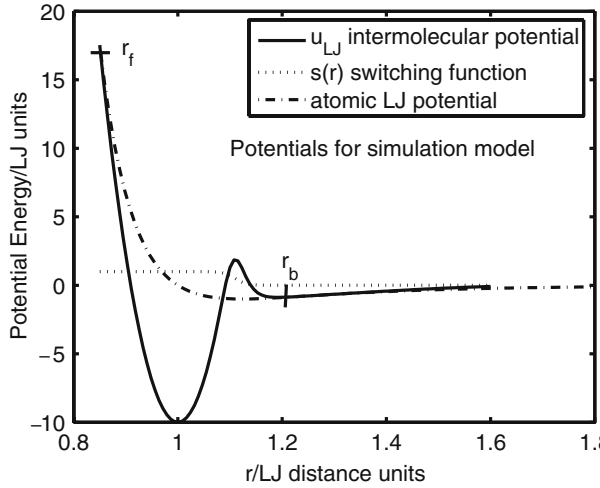

Figure 1. Potentials used for this work.

state configuration of figure 2 and the reduced distance model with the same spatial coordinates for the onset of the forwards and reverse reactions in figure 3. This is a typical reaction potential and it is proposed that a quantitative simulation of a simple dissociation reaction of a diatomic gas such as H_2 be attempted. It was found that the equilibrium exchange rate of equation 1 was very low at lower temperatures and changed rapidly at higher temperatures to a saturation level for the latter model (figure 3), not making it very suitable for studies where rates of formation and breakdown of bonds must be large enough for accurate statistics to be gained across the MD cell over a wide range of density

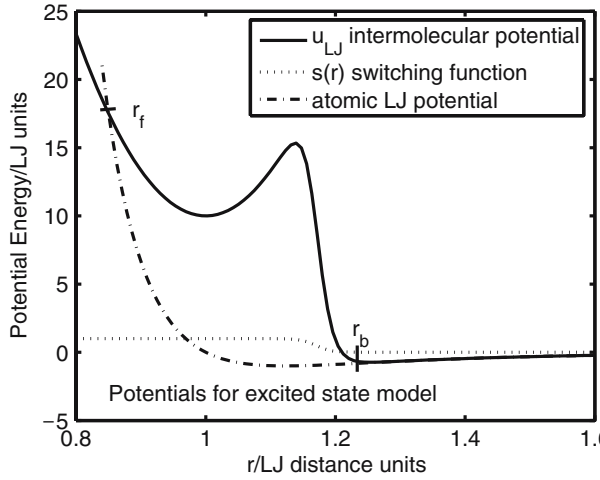

Figure 2. Potentials used for the excited molecular state.

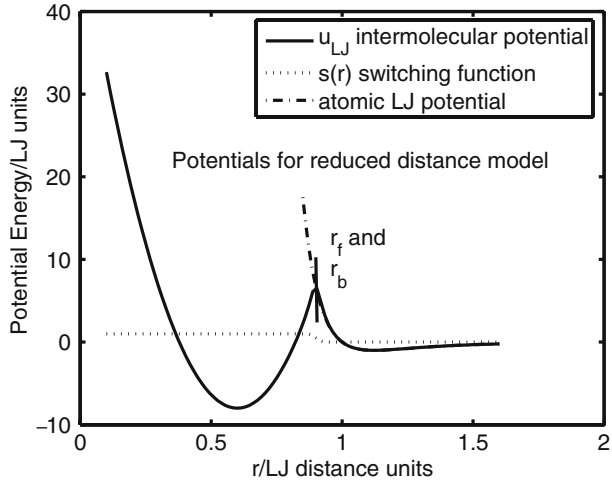

Figure 3. Potentials used for reduced distance molecular model.

and temperature ranges for a test system; the reason for the slow exchange is in part related to the small reaction or collisional cross-section of the molecule.

The MD mechanism for bond formation and breakup is as follows. The free atoms A interact with all other particles (whether A or A_2) via a Lennard–Jones spline potential and this type of potential has been described in great detail elsewhere [12]. An atom at a distance r to another particle possesses a mutual potential energy u_{LJ}, where

$$\begin{aligned} u_{LJ} &= 4\varepsilon\left[\left(\frac{\sigma}{r}\right)^{12} - \left(\frac{\sigma}{r}\right)^{6}\right] \quad \text{for } r \leqslant r_s, \\ u_{LJ} &= a_{ij}(r - r_c)^2 + b_{ij}(r - r_c)^3 \quad \text{for } r_s \leqslant r \leqslant r_c, \\ u_{LJ} &= 0 \quad \text{for } r > r_c \end{aligned} \tag{2}$$

and where $r_s = (26/7)^{1/6}\sigma$ [12]. The molecular cut-off radius r_c of the spline potential is such that $r_c = (67/48)r_s$. The sum of particle diameters is σ and ε is the potential depth for interactions of type A–A (particle–particle) or A–A_2 (particle–molecule) designated (1–1) or (1–2), respectively. The constants a_{ij} and b_{ij} were given before [12] as

$$\begin{aligned} a_{ij} &= -(24192/3211)\varepsilon/r_s^2, \\ b_{ij} &= -(387072/61009)\,\varepsilon/r_s^3. \end{aligned} \tag{3}$$

The potentials for this system is shown in figure 1. Any two unbounded atoms interact with the above u_{LJ} (1–1) potential up to distance r_f with energy E= $u_{LJ}(r_f)$ when the potential is switched at the cross-over point to the molecular potential given by

$$u(r) = u_{vib}(r)s(r) + u_{LJ}[1 - s(r)] \tag{4}$$

for the interaction potential between the bonded particles constituting the molecule where $u_{vib}(r)$ is the vibrational potential given by equation (6) below and the switching function $s(r)$ has the form given by equation (7). The LJ reduced units are used throughout this work unless stated otherwise by setting σ and ε to unity in the above potential description. The relationship between normal laboratory units, that of the MD cell and the LJ units have been extensively tabulated and discussed [12] and will not be repeated here. For the system simulated here with the potentials depicted in figure (1), the switching function is operative up to r_b, the distance at which the molecule ceases to exist, and where the atoms, which were part of the molecule interact with the (1–l) potential u_{LJ} like other free atoms; bonded atoms interact with other particles, whether bonded or free with the u_{LJ} (1–2) potential. The point r_f of formation corresponds to the intersection of the harmonic $u_{vib}(r)$ and u_{LJ} curves, and their gradients are almost the same at this point; by the Third dynamical law, momentum is always conserved during the crossover despite finite changes in the gradient, since the sudden change of the force field is between only

the two particles where the third law applies, thereby conserving momentum also. Total energy is conserved since the curves cross, and errors can only be due to the finite time step per cycle in the Verlet leap frog algorithm, which would cause the atoms to be defined as molecules at distances $r<r_f$. Similarly at the point of breakup, there is a very small ($\sim 10^{-4}$ LJ units of energy) energy difference between the LJ and molecular potentials despite using the switching function in the vicinity of the region to smoothen and unify the curves; the small energy differences at the cross-over points are less than that due to the normal potential cut-off at distance r_c where the normal (unsplined) LJ potential is used in MD simulations. In order to overcome this problem, a new algorithm (NEWAL) was developed, the details of which will be described in another work, which conserves momentum and energy at these two different types of cross-over points, where in one case, the switch is used (for breakup of the molecule) and not for the other during molecular formation. Briefly, if $E_p(r)$ is the inter-particle potential (energy) and $E_m(r)$ that for the molecule just after the crossover, the algorithm promotes the particles to a molecule and rescales the particle velocities of only the two atoms forming the bond from $\mathbf{v_i}$ to $\mathbf{v'_i}$ $(i = 1, 2)$, where $\mathbf{v'_i} = (1 + \alpha)\mathbf{v_i} + \beta$ such that energy and momentum is conserved, yielding $\beta = \frac{-\alpha(m_1\mathbf{v_1}+m_2\mathbf{v_2})}{(m_1+m_2)}$ (for momentum conservation) and energy conservation implies that α is determined from the quadratic equation $\alpha^2 qa + 2qa\alpha - \Delta = 0$ with $a = (\mathbf{v_1} - \mathbf{v_2})^2$, $q = \frac{m_1 m_2}{2(m_1+m_2)}$ and $\Delta = (E_p - E_m)$. Interchanging m and p allows for the same equation to be used for break-up of the molecule to free particles. For the simulations, success in real solutions for α for each instance of molecular formation is 99.9 and 100% for breakdown-where the Δ value in this instance is very small ($\sim 1.0 \times 10^{-4}$). In these simulations, we ignored the cases when there was no solution to the quadratic equation, meaning no molecules are allowed to be formed at all, and the interactions are of the (1–1) variety. This new algorithm coupled with shorter time step (from the typical 0.002* for low-energy non-reacting systems to 0.00005*) ensured excellent thermostatting, where the thermostating was carried out at the ends of the box only, as is the case in most real systems. It should be noted that this smaller time scale is not unrealistic as the temperature for this system is of the order of 20–30 larger than the usual values chosen, and so the translational kinetic energy of the particles would scale by the same order. In this equilibrium study, the MD cell (which is a rectangular box) is divided into 128 equal orthogonal layers in the x-direction, which is of unit length in cell units. In this method of boundary conditions [12], the first 64 layers to the midpoint along the x-axis are a mirror reflection about the plane parallel to the other two axis passing through this x-axis mid-point. The y and z-directions have length 1/16 each (cell units). This shape is chosen because non-equilibrium simulations will concentrate on imposing thermal and flux gradients along the x-axis, which would allow for more accurate sampling of steady state properties about this axis [13]. The layers that are mirror reflections about the midpoint plane are averaged for steady state thermodynamical properties, leading

to effectively 64 layers. With this algorithm, with only end wall thermostatting, we sample each of the layers for temperature and pressure changes, and find that the profiles are rather constant, as shown in figure 4. The heat supply term (per unit time) are zero to within the error of fluctuation of energy. Without the algorithm, (but with the same time step increment) the center of the effective cell (layer 32) would have a temperature T^* higher than that of the thermostatted end layers by over 2 units, and the heat supply term would be significantly negative, implying a virtual heating up of the system at the middle due to the potential differences due to the switches at the crossover points, which will not conserve energy due to the finite time step increment. The pressure too would be unrealistically higher at the center of the cell, which is unphysical. The algorithm above therefore is very effective in overcoming these problems. It should be noted that the uncertainty with regard to temperature for each of the layers would be about 10–100 times larger than the total system temperature, which is derived from averaging over every particle in the system, whether bonded or not. Prior to the implementation of this algorithm, each layer would be thermostatted to maintain a constant and uniform temperature and pressure profile (during the preliminary design). The non-synthetic thermostatting at only the boundaries of one direction of the cell approximates most physical systems; thermostatting each layer is used for heat of mixing studies but would not show the long-range fluctuational dynamics of energy transfer due to the thermostats, even if the noise levels are much lower. Further, for chemical reactions, there will be energy interferences due to the thermostatting of each layer, and so here, only the ends of the cell was thermostatted to eliminate any such effects, even if a greater uncertainty is introduced due to the long range bilateral transfer of energy from system to thermostat. It is found that the results of this study differs only by about 15% (for the equilibirum constant) to that found earlier when all

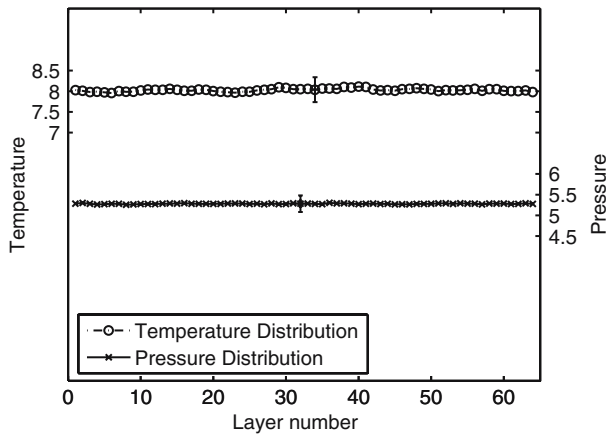

Figure 4. Pressure and temperature distribution across the MD cell.

the layers were thermostatted without implementation of the energy-momentum conservation algorithm. At regions $r < r_{sw}, s(r) \to 1$ according to (7) implying $u(r) \sim u_{vib}(r)$, i.e. the internal force field is essentially harmonic for the molecule and at distances $r > r_{sw}, u(r) \sim u_{LJ}$, so that the particle approaches that of the free LJ type as $r \to \infty$; the breakup is defined to occur at $r_b > r_{sw}$. Concerning the mechanism for the switching, in quantum mechanical kinetic descriptions, switch mechanisms are frequently used for describing potential crossovers [14], but from a classical viewpoint one can suggest that the inductive LJ forces due to the particle potential field (with particles having a state characterized by state variables $\mathbf{s}_{LJ}$) causes the internal variables at the critical distances and energies mentioned above to switch to state $\mathbf{s}_M$ when another force field is activated for the atoms of the dimer pair. State $\mathbf{s}_M$ reverts again to state $\mathbf{s}_{LJ}$ at distances r_b.

Incidentally, the shape of the potentials and switching mechanism used here is surprisingly similar to *experimental* discussions of the charge neutralization reaction [14]

$$K^+ + I^- \to K + I \tag{5}$$

except that the discussion does not explicitly mention the crossing over of the KI and K^+I^- potentials at short distances (high-energy) due to the "time-reversal" presuppositions referred to above. The existence of a cross-over would make the potential mathematically equivalent to the present treatment and there is good reason to suppose that such processes can and should occur in electromagnetically induced reaction pathways (such as is manifested in charge-transfer and Harpoon mechanisms) especially since the KI potential curve exists at shorter distances well before the crossover point. It is therefore postulated that there might well exist cross-over points not at the same vicinity for molecular formation and breakdown in actual reactions and that this simulation model is illustrative of such types of reactions. The following values were used here for the potential parameters:

(a) Current study (figure 1)
$u_0 = -10, r_0 = 1.0, k \sim 2446$ (exact value is determined by the other input parameters), $n = 100, r_f = 0.85, r_b = 1.20$, and $r_{sw} = 1.11$.

(b) Excited state model (figure 2)
$u_0 = 10, r_0 = 1.0, k \sim 2446$ (exact value is determined by the other input parameters), $n = 100, r_f = 0.85, r_b = 1.30$, and $r_{sw} = 1.17$.

(c) Reduced distance model (figure 3)
$u_0 = -8, r_0 = 0.6, k \sim 2446$ (exact value is determined by the other input parameters), $n = 100, r_f = 0.90, r_b = 0.90$, and $r_{sw} = 0.90$.

The intramolecular vibrational potential $u_{\mathrm{vib}}(r)$ for a molecule is given by

$$u_{\mathrm{vib}}(r) = u_0 + \frac{1}{2}k(r - r_0)^2. \tag{6}$$

A molecule is formed when two colliding free particles have the potential energy $u(r_{\mathrm{f}})$ whenever $r = r_{\mathrm{f}} < r_0$, at the value indicated in (a) above. This value can be defined as the isolated 2-body activation energy of the reaction and has the value of 17.5153 at r_{f}. A molecule dissociates to two free atoms when the internuclear distance exceeds r_{b} (which in this case is 1.20). The switching function $s(r)$ is defined as

$$s(r) = \frac{1}{1 + \left(\dfrac{r}{r_{\mathrm{sw}}}\right)^n}, \tag{7}$$

where

$$s(r) \to 1, \quad \text{if } r < r_{\mathrm{sw}},$$
$$s(r) \to 0, \quad \text{for } r > r_{\mathrm{sw}}.$$

The switching function becomes effective when the distance between the atoms approach the value r_{sw} (see figure (1)).

Some comments concerning the MD potentials are in order. It is generally not correct to assume that the potentials in figure (1) represents the TST potential surfaces; these surfaces can only be derived by computing the actual potential of the dimer or free atoms at a known internuclear distance in the presence of all the other species: the zero density limiting potentials of figure (1) cannot cause stable molecules to exist if they were formed by excited atoms with total kinetic in excess of the zero density activation energy since, if energy is conserved, the formed molecule would (except for a finite number of kinetic energy values, depending on the model) have to dissociate again to the atomic states from which they were formed initially. There must be energy interchange at the potential well of the molecular species to remove energy so as to prevent dissociation. This is achieved through the presence of the temperature reservoir. This reservoir, if it is coupled to the system would induce a system behavior whose limit at zero density would *not be* the same as an isolated mechanical system. Likewise, all standard states and other state functions of activation (free energy, entropy, etc.) must be computed as functions of all the coordinates of the particles involved in the interaction (including the reservoir). The numerical magnitude of these functions cannot be inferred only from the isolated potentials above, i.e. these potentials in conjunction with statistical mechanics should in principle yield the various system properties. Here, we extrapolate to zero density at fixed temperature to derive these functions, which cannot be inferred from mechanics only, nor from the potentials.

3. Thermodynamic results from equilibrium mixtures

The reacting mixture considered here were in thermodynamic equilibrium with 4096 particles. The cell was thermostatted at the ends of the cell maintained at the same temperature.

3.1. Determination of accuracy of computation and convergence

It will be observed that the results provided without any adjustments relatively smooth, even for this supercritical LJ system at relatively very high temperatures using nonsynthetic thermostatting of the systems at the boundaries of the cell only. Although this method is closer to many experimental situations where thermostats are located at the boundary of the system, the transfer of energy to and from any volume element within the system to the thermostats via the molecular and particle interactions would imply a greater fluctuation in kinetic energy and possibly other forms of potential energy than if each particle were individually thermostatted through a synthetic algorithm. As mentioned before, the algorithm (where a separate study will be presented) assures of flat temperature and pressure profiles with end-point thermostatting; just reducing the time step without implementing the algorithm was inadequate in ensuring the flatness of the $P - T$ profiles. The steps and criteria used to ensure adequate sampling with energy conservation were as follows:

(1) For the time increment selected, and for runs for a particular $(\rho, T)^*$ duple combination whose system properties were to be investigated in detail, the following had to obtain:

   (a) The heat supply to either of the reservoir had to have a standard error of fluctuation about zero that was (much) less that one standard error. The actual heat supply term in an NEMD experiment is typically several orders of magnitude greater. This ensures that there is overall energy conservation. It was found that this situation obtained for the $(0.7, 8)$ duple, which was used in testing out various properties. In particular, the run length was varied, as follows, at 3M, 4M, 6M, and 8M (where the set of values will be denoted $\mathcal{M}$) with the above criterion obtaining in each case of the set values. Hence the length of the run at 10M was chosen as a safe figure, where, incidentally, the above still obtained.

   (b) The P–T profile had to be flat for all these combination of conditions.

   (c) Properties of interest, especially the concentration equilibrium constant, rate constants and probability distributions were also viewed

at this particular duple value and for $\mathcal{M}$, and the variation was all within the vicinity of the errors given in the text for the duple concerned.

(2) For some of the algorithms, such as the ones for the diffusion coefficients, the maximum possible time prior to molecular breakdown was used (absolutely no extrapolation was attempted) in computing the coefficient from the Einstein expression, and so would be independent of $\mathcal{M}$ for large enough runs, (where the total duration of the molecule in general does not exceeding about $20,000$ units of δt^*), which means that there is no problem with the choices of $\mathcal{M}$ or 10 M. Likewise, for the probability distribution, the sampling is done at each 15th time step, and so depicts in general very low-scatter so as to be able to discern some features such as apparent temperature differences, as discussed in the sequel to this work.

Typical runs of 10 million time steps were performed per run at each general particle density ρ (where ρ is determined as a general density irrespective of whether the particle is free or is part of a molecule), where the first $200,000$ steps were discarded so that proper equilibration could be achieved for our data samples. The sampling methods have been previously described [12] where sampling of all data variables were done each 20th time step and where there were 100 dump values where each dump consists typically of 5×10^5 samples which are averaged. The 100 dump values are then averaged again to yield the standard errors of all variables. Dynamical quantities however had to be sampled at each time step $\delta t^* = 0.00005$. The thermostatting method conserves momentum and registers the energy absorbed at the thermostats [15]. All parameters given here are relative to LJ reduced units, sometimes denoted by $*$.

3.2. Equilibrium constants

There are two independent methods that are attempted here, both of which leads to the same results. The nonkinetic method (3.2.1) directly determines the concentration of reactants and products, and infers from these quantities K_{eq} at $T^*_{\mathrm{set}} = 8.0$, whereas the kinetic method (3.2.2) infers K_{eq} from taking ratios of the computed forward and backward rate constants at the same temperature.

3.2.1. Non-kinetic method

In order to find the thermodynamic equilibrium constant, K_{eq}, the following procedure was adopted. The concentration ratio, K_{c} defined as

$$K_{\mathrm{c}} = \frac{x_{\mathrm{A}_2}}{x_{\mathrm{A}}^2} \tag{8}$$

was determined as a function of average system density, ρ where the x's represent number density concentrations. For this and all other equilibrium quantities, the system temperature was set at $T^*_{\text{set}} = 8.0$, with the actual temperature fluctuating error of order $< 10^{-4}$. At very small densities, the system becomes an "ideal" mixture, but as mentioned previously, the limit of the potentials cannot be the same as the isolated potentials used in the MD calculations, since if this were the case, all the molecules would break up, yielding a net zero value for the equilibrium constant at the limit of zero density. As another project, it would be of interest to determine the limiting density and thermostatting time intervals at which the equilibrium regime breaks down in this system, and to elucidate the theory when this occurs. There may well be technical difficulties involved in computations of very low-density systems though. The plot of $K_c = K_c(\rho)$ is shown in figure (5). The accuracy of the K_c values varies inversely with a function of ρ, where in the captions SD refers to the number of standard deviations of the standard error. At low-densities, fluctuations in K_c implies that any extrapolative method can be ruled out, unlike previously (when NEWAL was not devised) when all the layers were individually thermostatted and where a least squares fit n-order polynomial expansion $p(x) = \sum_{i=0}^{n} a_i x^i$ to derive the zero density limit of the concentration ratio was utilized; the value of n was between 2 and 4. The zero density limit K_0 where $K_0(T^*) = K_c(\rho \to 0)$ is the true equilibrium constant. It is clear that in this system K_0 and K_c in general differ significantly; it serves as a warning that in general, one cannot ignore activity coefficients in the calculation of such properties in model systems and theoretical demonstrations if semi-quantitative results are desired. In the present study, it was discovered that at very low densities, fluctuations are significant as shown in figure (6) for the case of a run at

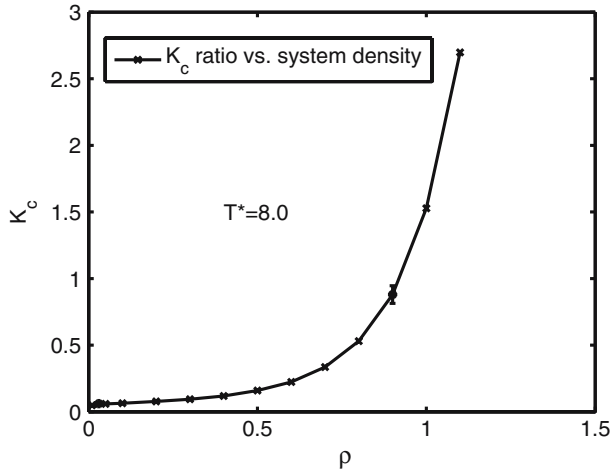

Figure 5. Variation of concentration ratio K_c with ρ, the system number density at LJ temperature $T^*_{\text{set}} = 8.0$ with SD = 3 at $\rho = .03$ and SD = 50 at $\rho = 0.7$.

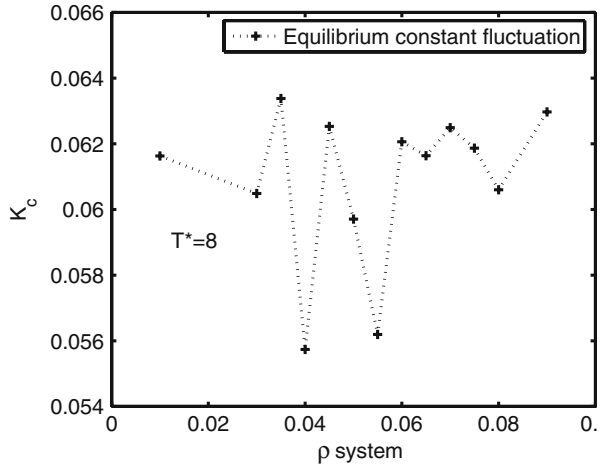

Figure 6. Illustration of fluctuation of individual runs at rarefied density state.

$T^*_{\text{set}} = 8.0$. The method used in the present case is to take the mean value of K_c for very low ρ values (rarefied state) ranging from 0.03 to 0.09, for about 12 values at any one temperature and to approximate this as $K_0(T^*)$. The fluctuations show that in this range of density, the system has "saturated" itself in that all the ρ values yield approximately the same mean K_c. Also, at such exceedingly low densities, one would expect a larger fluctuation in the determination of the rate values; nevertheless, we notice a saturation, with a maximum scatter of values for K_c of about ± 0.006.In view of the fact that at much higher densities, the absolute change of this constant is very much greater for unit change of density, the errors are still relative not large. The results derived for $T^* = 8.0_{\text{set}}$ are

$$K_{\text{eq}}(T) = \lim_{\rho \to 0} K_c(T) = 0.0610 \pm 0.002 \text{ LJ units.} \tag{9}$$

In previous studies prior to NEWAL implementation, using polynomial extrapolation, a value of $0.050 \pm .001$ was derived. However, these two values, although close, need not coincide because the phase-space trajectory of the two systems are not the same theoretically, meaning they are not the "same" chemical reaction system, even the only alteration here involves the time step and the thermostatting of each layer. (A change in the time step increment would alter the phase-space trajectory; so would the thermostatting mechanism.) Knowing $K_{\text{eq}}(T)$ from (9), which is an invariant quantity for any one temperature, the activity coefficient ratio, Φ can be calculated for the other densities at the same temperature by using

$$K_{\text{eq}} = K_c \frac{\gamma_{A_2}}{\gamma_A^2} = K_c \Phi. \tag{10}$$

The ratio of activity coefficients Φ is shown as a function of density in figure (7).

It is clear from the Φ ratio that for normal densities, the equilibrium reaction mixture is highly nonideal, which may be expected due to the large differences in the LJ energy well for the molecule and the atom (see figure (1)). It is probably a poor approximation to use ideal models for test systems in reactor design, which is often the case. Further, the above technique allows for the general determination of activity coefficient ratios via simulation. The determination of separate activity coefficients is a challenge. One real problem is the fact that molecules, in the *equilibrium* state cannot exist in isolation. In mixtures, either the reaction goes to completion, or they do not react, as in the simple theory of mixtures. In the latter case, one might postulate separate ideal states for the "pure" components, but in the present elementary case, for any one temperature, there is a finite value for K_0 meaning the presence of all components in a system at equilibrium. It it therefore a challenge to find a suitable model or concept to solve this problem with cycle changes. Even if a hypothetical state were defined, one must still design the route or cycle taken to the equilibrium state, which consists of product and reactant species. The derivation would require a series of very elaborate and detailed computations and is not attempted here since, it is not immediately relevant. Nevertheless, from the equilibrium distribution at various temperatures, the standard enthalpy, entropy and Gibbs free energy can be computed. Traditionally, many have interpreted these quantities as reflecting function changes for "pure" component reactants to pure molecular product without any simultaneous presence (or equilibrium) between the two.

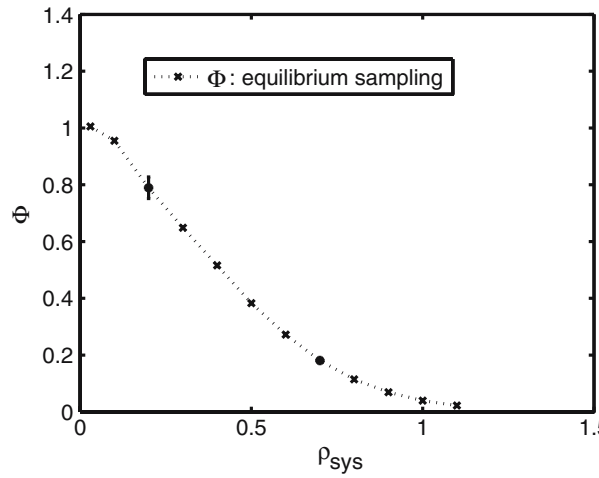

Figure 7. Variation of Φ with ρ, the system number density at LJ temperature $T^*_{\text{set}} = 8.0$.

3.2.2. Kinetic rate method

The rate constant is a defined quantity, with the standard form below. The overall rate of reaction r may be written in terms of the experimentally determined forwards rate ($r_1 = k_1 x_A^2$) for the process $2\mathrm{A} \overset{k_1}{\rightarrow} \mathrm{A}_2$ and backwards rate ($r_{-1} = k_1 x_{A_2}$) for the process $\mathrm{A}_2 \overset{k_{-1}}{\rightarrow} 2\mathrm{A}$ as $r = r_1 - r_{-1} = k_1 x_{\mathrm{A}}^2 - k_{-1} x_{\mathrm{A}_2}$; k_1 and k_{-1} are the respective rate constants.

At equilibrium $r = 0$, and so

$$\frac{x_{\mathrm{A}_2}}{x_{\mathrm{A}}^2} = \frac{k_1}{k_{-1}}. \tag{11}$$

The ratio of rate coefficients is the concentration ratio K_c where

$$K_\mathrm{c} = \frac{k_1}{k_{-1}}. \tag{12}$$

To verify the above equilibrium constant independently from concentration measurements used in the previous section, one can extrapolate to zero density ρ the values for $r_1/x_{\mathrm{A}}^2 = Q = k_1$ and $r_{-1}/x_{\mathrm{A}_2} = R = k_{-1}$. The rates were calculated independently from the program by monitoring the number of bonds formed or broken for each time step δt^* and averaging this quantity over the 10M time steps. Then the relevant equations are

$$\lim_{(\rho \to 0)} \left(\frac{Q}{R} \right) = K_\mathrm{eq} = \frac{\lim\ Q(\rho \to 0)}{\lim\ R(\rho \to 0)} = \frac{Q^0}{R^0}. \tag{13}$$

The plots of Q and R at low-densities are given in figure (8).

As for the direct determination of the equilibrium constant from concentration measurements, fluctuations imply an averaging at very low-densities of

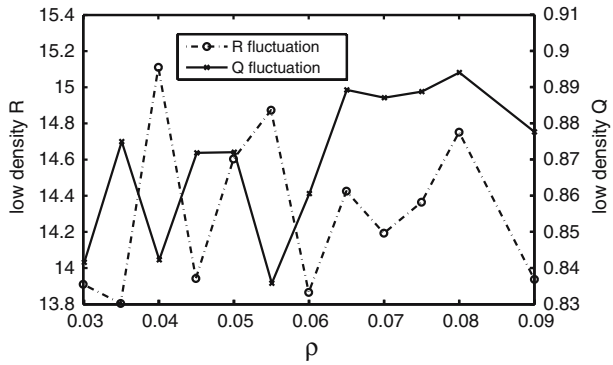

Figure 8. Values of Q and R variables at $T^*_{\mathrm{set}} = 8.0$ and at rarefied densities showing "saturation" behavior to a mean value as required by the limit theorems. At such low-densities, fluctuations are observed with an even scatter about the mean value.

the values given in the figures to derive the limits. The results with the estimated errors are

$$\langle Q\rangle_{\{\rho<0.09\}} = \lim_{\rho\to 0} Q \;=\; Q^0 = 0.870 \pm 0.006\,\text{LJ units}, \tag{14}$$

$$\langle R\rangle_{\{\rho<0.09\}} = \lim_{\rho\to 0} R \quad = R^0 = 14.32 \pm 0.1\,\text{LJ units}. \tag{15}$$

It will be noticed that at very low-densities, we would expect the errors due to the breakdown process to be very much higher than that due to the formation process since, the number of dimers tends to a low number and this is reflected in the R^0 uncertainty.The ratio of the values given in (14 and 15) gives the true equilibrium constant according to (13) where

$$K_{\text{eq}}(\text{kinetic}) = \lim_{\rho\to 0} \frac{k_1}{k_{-1}} = 0.061 \pm .001\,\text{LJ units}. \tag{16}$$

This kinetically derived result is in excellent agreement with the results from the previous method. The agreement indicates that the system is in a steady (equilibrium) state and that the simulation method is fairly coherent. The Q and R functions at other densities are given in figure (9).

3.3. *Standard states*

We use the form $\Delta G^0(T) = -kT \ln K_{\text{eq}}$ to determine the standard free energy state $\Delta G^0(T)$ of the dimer reaction. The justification is that, we can choose the standard state to be at constant pressure (of zero value) for the standard state, implying that the chemical potential standard state for each species

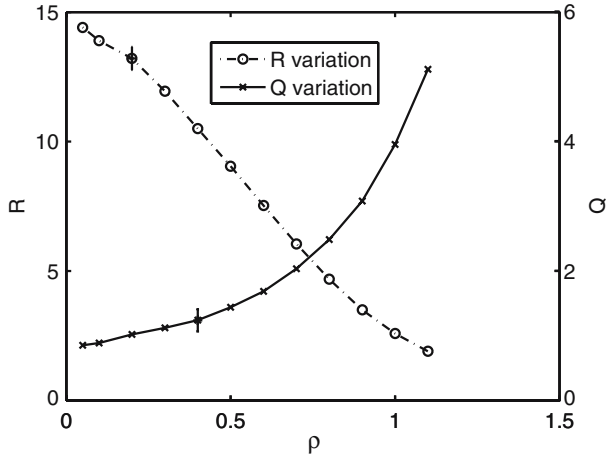

Figure 9. Variation of Q and R variables with density at $T^*_{\text{set}} = 8.0$.

is only a function of temperature, so that $\Delta G^0(T)$ is strictly only a function of temperature [16, pp. 177–179]. We repeat the same process as described above in section (3.2) for $T^*_{\text{set}} = 8$ for different temperatures (from $T^* = 4 - 20$). Each determination required at least eight runs at varying low-densities. It was found that at low-temperatures, the fluctuations were greater, as shown in figure (10) where the variation of K_{eq} versus $1/T$ is given. The linearity of this curve can also be used to derive an average value for each of the quantities calculated below for the entire temperature range. The curve used to determine the other standard state functions was the Gibbs free energy curve, given in figure (11). For this curve, the error bars (except for the first data set) all refer to the errors relative to the least squares fit of a quadratic curve to the simulation result. The fit is rather good. The standard entropy $\Delta S^0(T)$is derived from the thermodynamical entity [16, equation 6.34, p.182]

$$\frac{\mathrm{d}\Delta G^0(T)}{\mathrm{d}T} = -\Delta S^0(T). \tag{17}$$

Clearly to use (17), we must know $\Delta G^0(T)$as a function of temperature T. We write therefore a simple quadratic equation with p coefficients as follows

$$\Delta G^0(T) = p(1)T^2 + p(2)T + p(3). \tag{18}$$

The non-linear least squares method yields $p(1) = -0.0233441$, $p(2) = 1.0531305$, $p(3) = 15.46544989$ with an overall uncertainly of the free energy as approximately ± 0.3. Differentiating (18) yields the entropy as $\Delta S^0 = -(2p(1)T +$

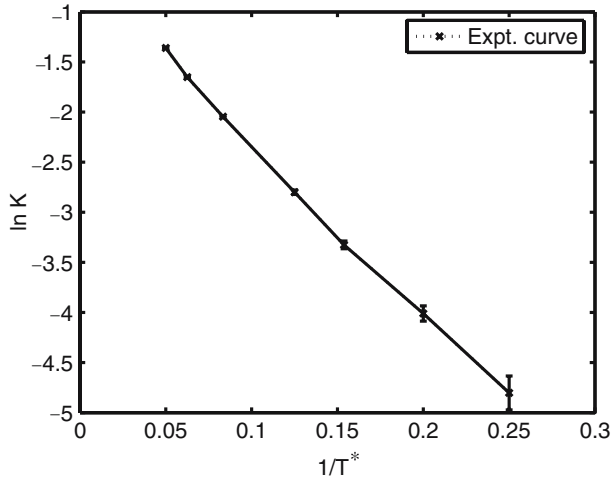

Figure 10. Variation of equilibrium constant K_{eq} with $1/T$ for fixed average system $\rho = 0.70$ with best fit line.

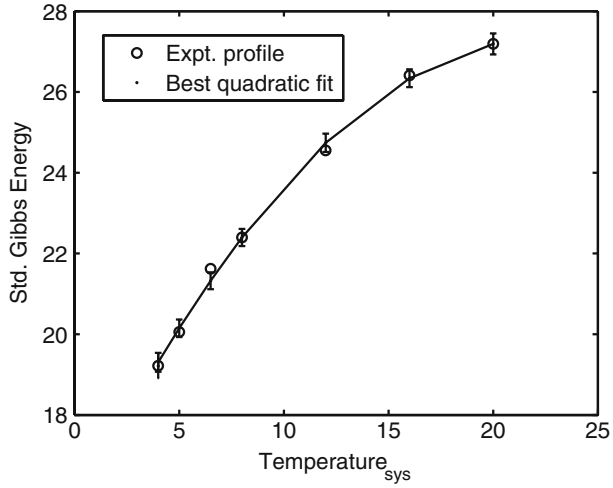

Figure 11. Variation of the standard Gibbs free energy ΔG^0 with temperature.

$p(2)$), which is linear. The standard enthalpy ΔH^0 is given at constant temperature by the entity [16, p. 183]

$$\Delta H^0(T) = \Delta G^0 - T\Delta S^0, \tag{19}$$

which therefore means that the standard enthalpy is given by $\Delta H^0 = -p(1)T^2 + p(3)$. It can be verified that this expression and that for ΔS^0 recovers the quadratic (18).

The plots for the standard entropy and enthalpy as functions of temperature are given in figure (12).

Most experimental methods take gradients to yield average values of the standard states over a temperature range. Here, the explicit values can be

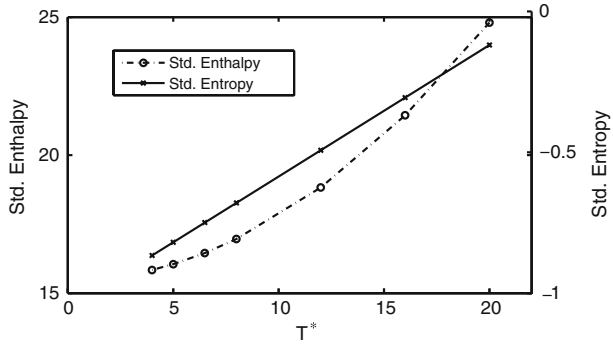

Figure 12. Plot of standard enthalpy $\Delta H^0(T)$ and entropy $\Delta S^0(T)$ from $\Delta G^0(T)$ quadratic curve fit with the temperature T^*.

calculated over the temperature range. From the calculations, we find that the standard entropy is negative, as it must be at moderate to low-temperatures since, the free particle state has a larger phase space than the corresponding dimer. It may appear counter-intuitive that the standard enthalpy is positive. It must be pointed out that at these temperatures, the particles are not trapped at the bottom of the potential well, and that the activation energy is positive, and that the internal potential energy at the point of formation of the molecule is not lost, but is converted to internal kinetic energy even up to the point of the break-up of the molecule, implying a positive value of this quantity relative to the dissociated particles. A quantitative treatment of these terms has been attempted [17]. It must be concluded that the simulations are able to determine the standard states without having to construct extremely detailed cycle diagrams; further, the simulation can also check on the correctness of the cycle diagrams used to determine standard state values.

3.4. Activation energies

From the way the algorithm was constructed for molecular formation, the molecularity of the elementary reaction is two leading to a single second-order reaction of formation, and for the dissociation of A_2, a first-order reaction results since, the molecule is only allowed to exchange kinetic energy with all other particles within the system without further reactions to the dissociation limit. A frequently used model for the kinetic constant k_i for these rates is due to Arrhenius, which has the form

$$k_i = A_i \exp\left(-\frac{E_i}{\mathrm{RT}}\right), \tag{20}$$

where the rate constant is a function of the temperature only and where A_i is ideally not temperature dependent. It should be noted that the Arrhenius equation is strictly valid for 2-dimensional systems where the pre-exponential factor is independent of temperature and where the exponential factor $\exp\left(-\frac{E_i}{\mathrm{RT}}\right)$ represents the fraction of molecules having energy in excess of E_i [18], where E_i is usually understood to be the activation energy. The reason why this form is so durable is that the exponential term represents the fraction of excited state atoms, and this term dominates over the pre-exponential term with temperature variation, which give the impression of constant A_i factor for the plots. The rate constants for the forward k_1 and reverse reaction k_{-1} were plotted versus $1/T$ for the given density of $\rho = 0.7$ and was found to be reasonably linear figures (13 and 14), with the activation energies for the forwards and the backwards

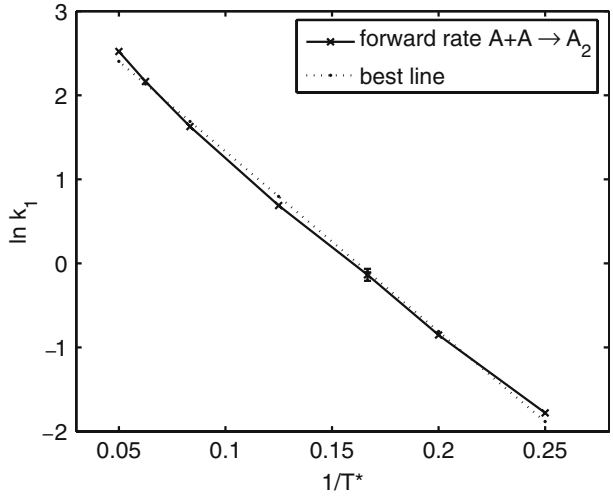

Figure 13. Variation of natural logarithm of forwards (product forming) rate constant k_1 with reciprocal of temperature for $\rho = 0.7$.

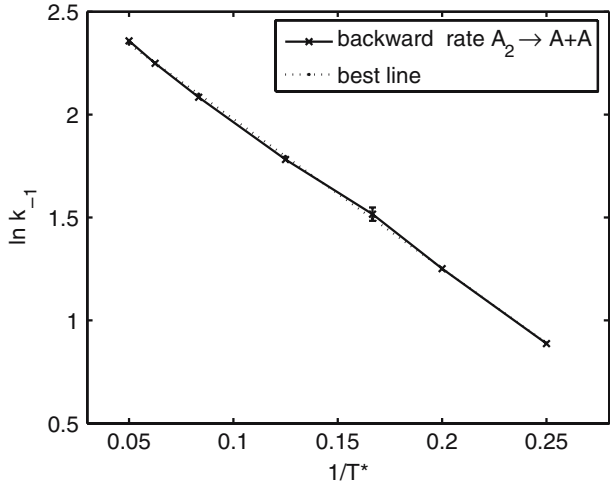

Figure 14. Variation of natural logarithm of backwards (product disintegration) rate constant k_{-1} with reciprocal of temperature for $\rho = 0.7$.

reaction rates (E_1 and E_{-1}, respectively), and the corresponding collision factors (A_1,A_{-1}) determined approximately as

$$E_1 = 21.40 \pm 0.10 \text{ LJ units}, \qquad A_1 = 3.50 \pm 0.2 \text{ LJ units}.$$
$$E_{-1} = 7.26 \pm 0.02 \text{ LJ units}, \qquad A_{-1} = 2.70 \pm 0.04 \text{ LJ units}.$$

There are two separate rate constants here, for first and second-order. The second-order forwards rate constant k_1 has a form given by

$$k_1(T) = \pi b_{\max}^2 \left(\frac{8kT}{\pi\mu}\right)^{1/2} \exp\left(-\frac{\epsilon^*}{kT}\right) = A_1 \exp\left(-\frac{\epsilon^*}{kT}\right) \tag{21}$$

according to "simple collision theory" (SCT). Very roughly, if the mean temperature for the plot (which spans from 4 to 20) is 12, then (21) above yields for the given value of $A_1, b_{\max} = 0.9153, \ldots,$ which is reasonably close to 0.85, the theoretical value. However, $\epsilon^* = 21.40$, which is higher than 17.5153, which is the set simulation potential value for the formation of a molecule. Since, we can expect a yet greater accuracy for the determination of ϵ^* as compared to A_i due to the domination of the exponential terms, it may be safe to suppose that other factors contribute to the true activation energy other than what is described by SCT. Future work will attempt to determine what other energy factors are implicated in ϵ^*; currently, SCT views this energy as a pure mechanical work energy, which obtains at the molecular level. Similarly, variation of A_i with various energy terms cannot be immediately ruled out. Generally, the above values do not bear a direct relationship to the isolated 2-body potentials of figure (1), but nevertheless some approximate correlations are evident; E_1 is somewhat close to the isolated activation energy 17.5153 measured from the free atomic states, and likewise E_{-1} is somewhat close to the energy difference from the bottom of the molecular potential at -10 to the potential at r_b, a distance of approximately -9 energy units. However, for a first-order reaction, a different interpretation for energy differences obtain than that due to SCT, which is concerned with bimolecular processes; the first-order interpretation is that the molecule decomposes when it overcomes an energy activation threshold, and the fraction of such molecules is reflected in the exponential term, the pre-exponential term reflecting the mechanism of the decomposition.

4. Results from equilibrium dynamical trajectory analysis

This section concentrates on variables, which had to be sampled at each time step of duration $\delta t = 0.00005^*$ in order to compute the property of interest: the rate of reaction in the previous section above is also based on instantaneous sampling but more properly belongs to topics associated with equilibrium. Of importance in nonequilibrium and kinetic studies are the values of the diffusion coefficients, reaction correlation coefficients and the energy probability distributions, where if the principle of local equilibrium (PLE) obtains imply that we may approximate the values computed in an equilibrium simulation for those in a nonequilibrium volume element having the same state variables. Examples of these quantities (which can also gauge the appropriateness of the model for nonequilibrium studies) are provided.

4.1. Rotational diffusion constants

Although connected in some ways to diffusion, a somewhat unconventional 'reorientation' diffusion function $\langle \cos \phi(t) \rangle$ has been defined [6] where $\phi(t)$ is the angle *between* $\hat{\mathbf{R}}(0)$, the unit internuclear distance vector of the dimer at $t = 0$, and $\hat{\mathbf{R}}(t)$, the same unit vector at time t. Such a definition might have applications in conjunction with their being part of transform functions [6, equations (17)–(20), p. 211], where the postulated exponential decay of this function when acting as a kernel of the transform could force convergence of the function being convoluted. It is found that the exponential decay assumption in $\cos(\phi(t))$is a fair but not perfect fit, perhaps implying that another type of theory for "rotational diffusion" constants may yield even better fits with the experimental curves. We provide one such example $\langle \arccos(t) \rangle$, an approximation to $\langle \theta(t) \rangle$, which provides a far better fit and therefore is a candidate for another area of research in stochastic theory of rotational diffusion. It must be mentioned, however, that the theory of "rotational diffusion" as developed by Debye [19, pp. 81–84, esp equations 49], etc. makes use of "dissipation kinetics" where a constant torque M is balanced by a inner frictional force ζ parameter, so that $M = \zeta \frac{\mathrm{d}\theta}{\mathrm{d}t}$, where θ is an angular displacement. Such a theory leads to a relaxation in the distribution function f by a factor $\varphi(t)$ given by $\varphi(t) = \exp -\frac{2kT}{\zeta} t$ so that for a particular orientation angle θ, f has the form $f = A[1 + C\varphi(t) \cos \theta]$. The mean dipole moment of the entire sample also decays with the same rate as with φ. It is not immediately clear that the orientation angle must also relax according to a first-order rate law. If the effect is a projection of an orientation onto an axis, then this would correspond to the result given by Allen (op cit). O'Konski and Haltner [20] have characterized TMV (a virus) by studying the birefringence relaxation rate written $\delta = \delta_o \exp(-t/\tau)$ where τ_o is the initial value of birefringence [20, equation 3, p. 3607] and the "rotational diffusion coefficient" D_h is defined here as $D_h = 1/6\tau$ with an additional factor of 1/3 compared to that of Allen. Most of these theories supposes that even at the molecular level, one can use frictional coefficients as for macroscopic systems where the retarding force is linearly proportional to some form of velocity of the system, the constant of proportionality involving the frictional coefficients [21]. More recent experimental studies of rotational diffusion [22,23] assume a first-order relaxation of fluorescent directed intensities of the chromophore of the molecule with the rotational diffusion constant defined as in [20]. To show that the results obtained is typical, we graph the functions as defined by Allen [6]. The method used here to determine $\langle \cos \phi(t) \rangle$ is to create a table whenever a molecule is formed, which maps out for each increment in the time step i the value of $\cos \phi(i)$ until it disintegrates: for each ith time step there exists for each sampling subinterval M (M being a variable) values of $\phi(i)$ due to other molecules, which have existed, and the average value for each sub-interval is computed

as $\langle \cos\phi(i) \rangle = \sum_{j=1}^{M} \cos\phi_j(i)/M$. According to Allen (op cit), the function decays as

$$\langle \cos\,\phi(t) \rangle = A \exp(-t/\tau_1)\ (A = 1)$$

with linearized form

$$\ln\left(\langle \cos\phi(t) \rangle\right) = -t/\tau_1, \tag{22}$$

where the "rotational diffusion" coefficient D_r is given by $D_r = \frac{1}{2\tau_1}$. The results of the simulation is graphed in figures (15–17). Figure (15) graphs the proposal found in [6]. It is clear that there is an initial chaotic regime, followed by a very slow decay of approximate form $A \exp(t/\tau_r)$,$(A = 1)$ if we measure the time from the end of the chaotic regime onwards; fitting this portion of the curve from the 400th to 800th time step to the above exponential yields $\tau_r = 1.38 \pm 0.02$ LJ units. A "rotational diffusion constant" $D_r = \frac{1}{2\tau_r}$ may be defined and the value obtained is $D_r = 0.36 \pm 0.01$ LJ units. The shape of the $\langle \cos\phi(t) \rangle$curve resembles that described in [6] (where the "initial chaotic region" is mentioned) implying a somewhat typical rotational motion, but it is clear from the figure that even in the fitting region, there is an apparent concave shape, as the tangent line makes clear. Nevertheless, for the sake of parametrization, this particular definition is used to derive the diffusion constant D_r data at other regimes of varying ρ (at constant temperature) in figure (17) and for varying temperature (at constant ρ) as depicted in figure (16), all of which are determined from the gradient between the 400th and 800th time step, i.e. in these figures, the same method of determining D_r was used as for the above determination of

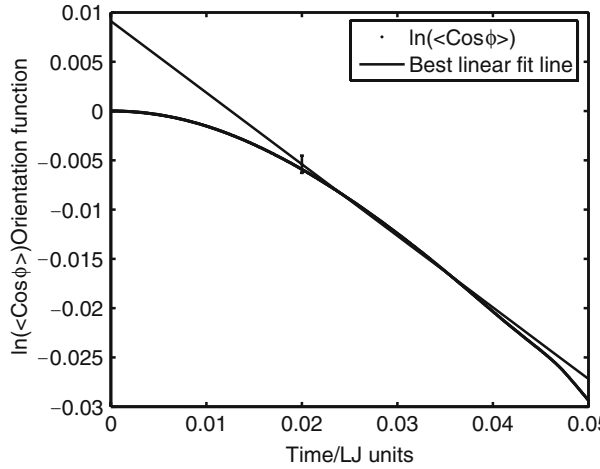

Figure 15. Variation of natural logarithm of cos ϕ orientation function with time at $T^* = 8.0$ and $\rho = 0.7$.

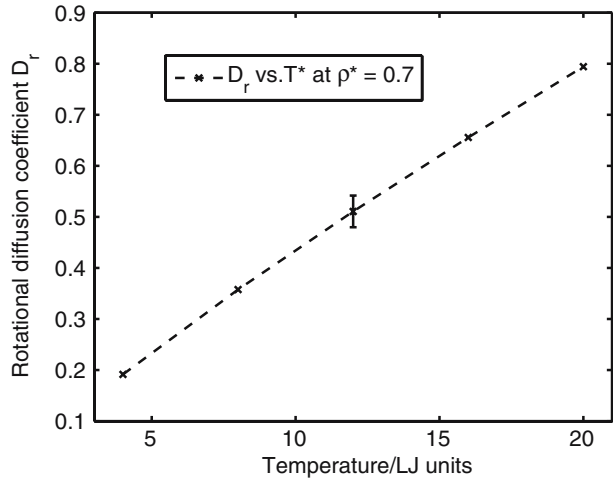

Figure 16. Variation of D_r with temperature at constant $\rho = 0.7$.

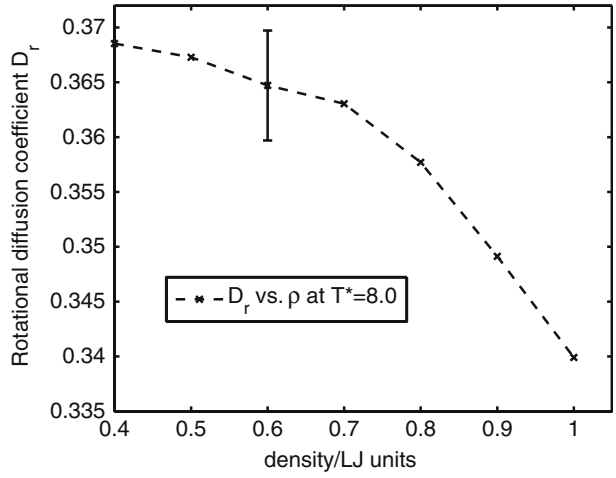

Figure 17. Variation of D_r with density at constant temperature $T^* = 8$.

D_r at $\rho = 0.7$ and $T^* = 8$. As with the case of rectilinear diffusion motion $D_t = BkT$, where B is the density dependent mobility coefficient, which is the steady state velocity acquired per unit external force [24, section 14.4, equations (2–11), pp. 464–465], we obtain at fixed density ρ a linear relationship with temperature, suggesting a similarity or isomorphous theoretical construct in relation to rotational motion. Noting that different thermodynamical variable regimes are associated with different error margins when determined experimentally, we also notice an approximate linear correlation with density at fixed temperature. From the rectilinear equation, this would be the case if the mobility coefficient B were

inversely linearly related to the density of the medium, which is a very reasonable assumption at higher densities ($\rho^* = 0.75-1.0$). The figures show that the change of the diffusion constant with ρ at fixed temperature is much less dramatic than with temperature at fixed ρ.

Figure (18) gives a clear indication that the long-time correlation concerning time and the logarithm of θ shows a very good linear fit (i.e. $\ln\theta$ versus t), and so one can also derive a rotational diffusion coefficient where the actual angular distance relaxation is a first-order process by creating an appropriate theory as suggested by computations (at least for the model adopted here.) Lynden-Bell [25] has written an extensive review of the theoretical underpinnings of molecular reorientations; she concentrates on the concept of angular momentum as an indicator of reorientations. Many possibilities present themselves concerning the reorientation correlation function relaxation in time, which has the form $C_{J\alpha}(t) = \langle \mathbf{J}_\alpha(t) \mathbf{.} \mathbf{J}_\alpha(0)\rangle / \langle \mathbf{J}_\alpha(0) \mathbf{.} \mathbf{J}_\alpha(0)\rangle$ with α denoting the orientation with respect to a particular molecular axis. $\mathbf{J}_\alpha$ denotes the angular momentum about the designated axis of rotation. This $C_{J\alpha}(t)$ correlation function can have an exponentially decaying form if the Fokker–Planck or J diffusion model is used, but this is one of several possibilities [25, figure 1, p. 503] but for this dimer (a linear molecule), an exponential decay (linear in $\ln(C_{J\alpha})$ may be expected, where the angular velocity ω correlation is identical to $C_J(t)$. Here we note a long time linear correlation with $\ln\theta(t)$ and not its derivative. It could very well be that if the actual angular momentum were monitored, then an exponential decay with time would be observed in the current model, or that relative to those theories which predicts an exponential decay with the ω correlation function, the current result for the evolution of $\theta(t)$ is in accordance with it; if not, then another the-

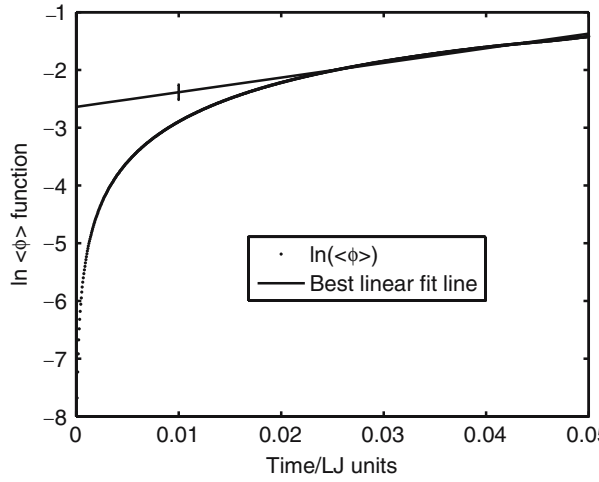

Figure 18. Variation of natural logarithm of arccos(cos ϕ) orientation function with time at $T^* = 8.0$ and $\rho = 0.7$.

oretical approach may be feasible, complementing those given by others, such as Steele or Powles [25, Conclusions, p. 517] and the many others since that time.

4.2. Self-diffusion coefficients

In these simulations, the mean lifetime of the molecules vary broadly in the region of 24,000–2,400 time steps as the corresponding temperature varies from $T = 4.0$ to $T = 8.0$. The accurate determination of the three dimensional (3-D) self diffusion coefficient D_s for any particle requires the determination of the integral of the long time limit of the velocity autocorrelation function, or the equivalent Einstein expression of the mean square displacement at infinite time with respective forms

$$D_{\mathrm{s}} = \frac{1}{3}\int_0^{\infty} \mathrm{d}t \, \langle \mathbf{v}_i(t) \cdot \mathbf{v}_i(0) \rangle \,, \tag{23}$$

and

$$2t D_{\mathrm{s}} = \frac{1}{3}\left\langle |\mathbf{r}_i(t) - \mathbf{r}_i(0)|^2 \right\rangle \; (t \to \infty), \tag{24}$$

respectively. We overcome the infinite time problem here by determining the diffusion coefficient according to (24) at the time of breakup $t_{\mathrm{br,i}}$ of molecule i (where the time is 0 when the molecule is formed), thus allowing for the maximum time possible before $D_{s,m,i}$ is computed (where m refers to the dimer.) Likewise, we can monitor the time spent as a free particle of any labeled atomic species (j), and determine the self diffusion coefficient $D_{s,a,j}$ (where a refers to the atomic state). The molecular self-diffusion coefficient is the average of all molecules determined during the dump interval, and lastly the 100 dump values for the entire run is averaged to provide an estimate of uncertainty. Similarly, a labeled particle is used to determine the atomic diffusion coefficient based on the time spent as a free, nonbonded particle. The results for this supercritical fluid are given in figures (19 and 20). The curves in figure (19) appear very linear, verifying the formula $D_{\mathrm{s}} = BkT$, according to previously developed theories [26 equation (49)] especially at lower temperatures. In non–reactive systems with spherical particles, the Stokes–Einstein law for diffusion of species i in a liquid j of viscosity η_j is $D_{i,j} \approx \frac{kT}{6\pi\eta_j r_i}$. The viscosity is independent of density, and so very approximately, one might be able to interpret the reaction as one species A–A moving within the matrix of the other atomic species A where the Stoke's law for the force acting on each of the species are viscosity dependent, and obtains for both. Under this assumption and approximation, since the viscosity is independent of temperature, a first-order linear relationship with the temperature is predicted for both species, as observed. Furthermore, this result

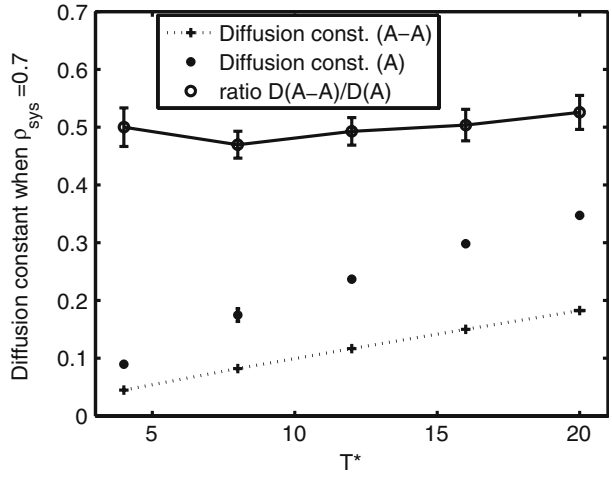

Figure 19. Self-diffusion coefficients at varying temperature and fixed $\rho = 0.7$, where A–A refers to the dimer and A to the atom, and D denotes the self diffusion coefficient.

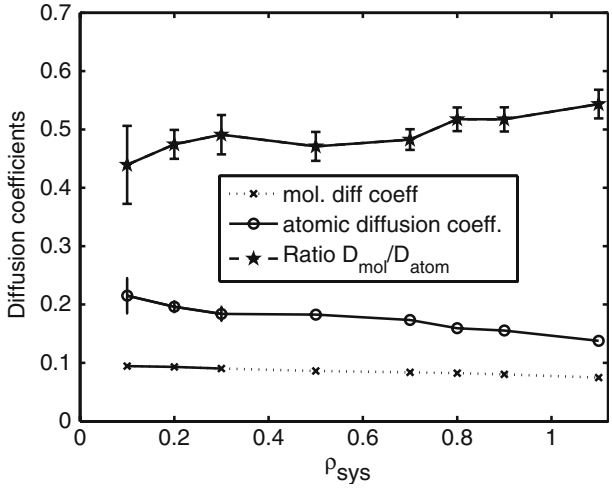

Figure 20. Diffusion coefficients at varying ρ and fixed $T^*_{\text{set}} = 8.0$.

is rather normal experimentally [16, p. 494, figure 16] for fluids (e.g. Ar(g) or $H_2O(1)$). The ratio of molecular to atomic diffusion constant is relatively close to 0.50 everywhere. The mass of the molecule is twice that of the atom and approximately twice the diameter, leading to this approximate ratio. The actual theoretical prediction due to size, energy interaction and mass effects is not well developed, and no extensive data are available for even non-reacting systems. The reactive system here depict values of the diffusion coefficient, which does not differ significantly for systems which do not react. In one study [27, p. 2044 Table 5]

of solute diffusion in a solvent, where interactions are solvent–solvent (1–1) and solvent–solute (1–2) only, (i.e. no (2–2) interactions) the L_2 system has the following Lennard–Jones parameters $\frac{m_2}{m_1} = 2$; $\frac{\epsilon_{22}}{\epsilon_{11}} = 4$; $\frac{\sigma_{22}}{\sigma_{11}} = 2$ leading to the diffusion coefficients $D_1 = 0.063$ and $D_2 = 0.017$ (accuracy not specified) and for the S_2 system, the Lennard–Jones parameters $\frac{m_2}{m_1} = \frac{1}{2}$; $\frac{\epsilon_{22}}{\epsilon_{11}} = \frac{1}{4}$; $\frac{\sigma_{22}}{\sigma_{11}} = \frac{1}{2}$ lead to the diffusion coefficients $D_1 = 0.082$ and $D_2 = 0.190$. For the same mass ratio, the diffusion constant ratios vary from 0.27 to 0.43 for very different and extreme (ϵ σ) combinations where the variation with temperature is not significant for these ratios based on the scanty information of the graphs drawn; however, for the work of this paper, $\epsilon = 1$, and $\sigma = 1$ throughout. The ratios from the above literature are not too different from the ones reported here. The variation of the diffusion constant with density is much less dramatic than for the temperature according to Figure (20) with a slight decline in diffusion constants with increasing density, as is to be expected as the mobility would decrease. The errors appear large because the variation of the coefficients with varying density is relatively slight for fixed temperature unlike that for the variation with temperature. Resorting again to the Stokes–Einstein equation with the presuppositions above, we would expect at constant temperature for there to be no change; the variation is due to the fact that the two fluids do not approximate as two fluids where one fluid serves as a solvent for the other. For hard spheres, the self diffusion coefficient varies inversely with the density of the gas. If this is another effect, combining this with the Stokes–Einstein expression and its assumptions above would lead to the prediction of a weak inverse dependence of the diffusion coefficient with density, which is precisely what is observed. Figure (19) yields the dimer (A–A) diffusion coefficient as ≈ 0.09 and the atomic (A) self-diffusion coefficient as ≈ 0.18, which is very close to the mean value found in the graph of figure (20). It appears that first-order kinetic theory, and the Maxwellian prediction of invariance of viscosity with density (pressure) is verified in these results.

4.3. Kinetic energy probability histogram

The potentials described in equations (2–7) have the form

$$\mathcal{H} = \sum_{i=1}^{m} p_i^2/2m + \sum_{i<j} V(r_i - r_j) \tag{25}$$

together with switches operating to determine the type of potential operating. This difference might conceivably alter the Gibbs postulate in the following manner. One of the postulates states that the time average of a particular system equals the ensemble average. The density-in-phase ρ corresponding to the probability of a particular state is given by $\rho \propto \exp -\beta\mathcal{H}$ and so the kinetic energy of any particle would be Boltzmannized for any particular system and therefore, if

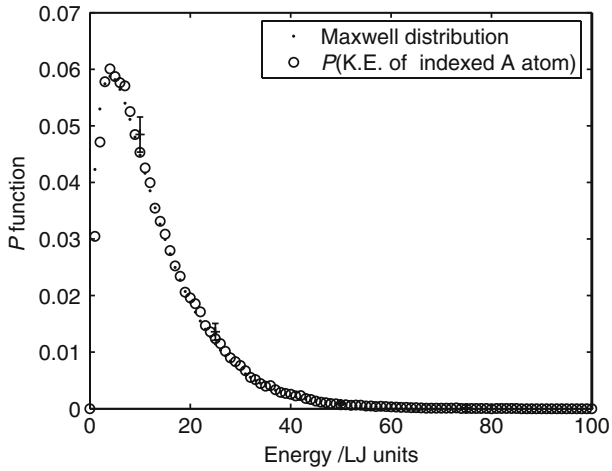

Figure 21. P functions for kinetic energy of fixed indexed atom A which either is bonded to some A_2 dimer or not at system temperature $T^*_{\text{set}} = 8.0$ and $\rho = 0.7$ with apparent temperature of atom $\langle T \rangle_{\text{atom}} = 8.1 \pm 0.2$. The uncertainty here is three standard error units.

a labeled particle is monitored throughout the whole simulation, from the time it is bonded and when it is not, then the above postulate demands a Boltzmannized kinetic energy distribution. The Gibbs postulate can be directly tested for the chemical reaction system to verify whether or not the switching mechanism modifies or contradicts the Gibbs postulate. Experimentally, (figure (21)), it is found that switches that leads to nonsingle-valued Hamiltonians *does not* affect the Gibbs postulate. If this postulate is valid for loop-like hysteresis systems, then the time trajectory of any indexed particle I must also yield, when averaged over a very long time the result (in 3-D) $3kT/2 = \overline{p_I^2/(2m_I)}$ whether the particle is bonded or not over the trajectory equally weighted for all the states that it traverses. The Maxwellian probability density function per unit energy increment is given by

$$P = 2\pi \left(\frac{1}{\pi} kT\right)^{3/2} \epsilon^{1/2} \exp - \left(\frac{\epsilon}{kT}\right). \tag{26}$$

Equation (26) is the standard form used for the absolute velocity distribution function since the energy $\epsilon \propto v^2$ for velocity v and this form tests for the Boltzmann distribution for kinetic energies. Noting that the accuracy of the single particle is reduced by a factor of ≈ 4000 (the number of particles in this simulation), we find that the Gibbs postulate seems to be verified in terms of the shape of the P function (which appears Maxwellian) as well as the computed value of the temperature with the error estimated as ± 0.1 by studying an atom of fixed label (no. 29) as it forms and breaks bonds with neighboring molecules, as shown in figure (21). Clearly, the time average of dynamical properties for this

particle would equal the ensemble average. We notice that the reduced accuracy of the sampling is reflected in the greater scatter of the P function points.

5. Conclusion

This study shows that the model of the molecule utilizing switching potentials does lead to typical behavior predicted from standard thermodynamics for unusual hysteresis-type reaction mechanisms, which theorists have largely ignored, due perhaps to the influence of "time-reversible" symmetry concepts. It is demonstrated that microscopic loop-like pathways does not influence the macroscopic thermodynamical results in any fundamental way. In particular, the Gibbs ensemble postulate is obeyed, implying that the thermodynamics is well-behaved.

The method used here to reduce expensive 3-body calculations to easier 2-body calculations may be used as a basis for nonequilibrium simulation applications, which will be the subject of further investigations. The two body potentials yield extremely good thermodynamic results whilst being super-efficient in reducing computational costs because the use of switches and algorithms that can preserve momentum and energy during potential transitions, and it is expected that semi-quantitative results at least can be determined for any known molecular potential. The NEWAL algorithm is effective for the extreme conditions of the simulation, and would prove to be a valuable tool in reducing errors attributable to switching potentials. This reduction in error would be even more evident at more "normal" conditions with the temperature parameter scaled 10–20 times less than those used here.

A whole generation of scientific literature has been devoted to establishing necessary connections between the direction of material flow (microscopic reversibility or "time reversibility") and thermodynamics, but the results here suggests that there need not be any necessary connection between the two. It would be of interest to repeat and compare some of the above calculations for a conventional system without hysteresis to rule out any necessary connection between dynamics and equilibrium thermodynamic properties.

Acknowledgments

C.G.J would like to thank (a) University of Malaya, Kuala Lumpur for financing a sabbatical visit to NTNU (2000–2001), and (b) availability of Intensification of Research in Priority Areas (I.R.P.A) grant no. 09-02-03-1031 from the Malaysian Government which was used to finance the computer system for the project and for conference and research visits to Europe and America where portions of this work were discussed [28].

References

[1] D.N. Hendrickson, Single-molecule magnets, in: *Abstracts of Papers, 225th ACS National Meeting 2003* (American Chemical Society, Washington DC, 2003).
[2] D. Gatteschi, From molecular magnets to magnetic molecules, Actual. Chimique. 6 (2001) 21–26.
[3] E. Sanudo, E. Carolina, W. Wernsdorfer, K.A. Abboud and G. Christou, Synthesis, structure, and magnetic properties of a Mn_{21} single-molecule magnet, Inorg. Chem. 43(14) (2004) 4137–4144.
[4] C.G. Jesudason, I. Time's Arrow, detail balance, Onsager reciprocity and mechanical reversibility: Basic Considerations, Apeiron 6(1–2) (1999) 9–24.
[5] C.G. Jesudason, II. Time's Arrow, detail balance, Onsager reciprocity and mechanical reversibility: Thermodynamical Illustrations, Apeiron 6(1–2) (1999) 172–185.
[6] M.P. Allen and P. Schofield, Molecular dynamics simulation of a chemical reaction in solution, Mol Phys. 39(1) (1980) 207–215.
[7] Y. Zeiri and E.S. Hood, Nonequilibrium distributions in reactive systems, Phys. Rev. Letts. 55(6) (1985) 634–637.
[8] J. Gorecki and J. Gryko, Molecular dynamics simulation of a chemical reaction, Comput. Phys. Commun. 54 (1989) 245–249.
[9] F.H. Stillinger and T.A. Weber, Molecular dynamics simulation for chemically reactive substances. fluorine, J. Chem. Phys. 88(8) (1988) 5123–5133.
[10] I. Benjamin, B.J. Gertner, N.J. Tang and K.R. Wilson, Energy flow in an atom exchange chemical reaction in solution, J. Am. Chem. Soc. 112 (1990) 524–530.
[11] J.P. Bergsma, J.R. Reimers, K.R. Wilson and J.T. Hynes, Molecular dynamics of the A+BC reaction in a rare gas solution, J. Chem. Phys. 85(10) (1986) 5625–5643.
[12] B. Hafskjold and T. Ikeshoji, Partial specific quantities computed by nonequilibrium molecular dynamics, Fluid Phase Equilibr. 104 (1995) 173–184.
[13] C.G. Jesudason, The Clausius inequality: implications for non-equilibrium thermodynamic steady states with NEMD corroboration, Nonlinear Anal. 63(5–7) (2005) e541–e553.
[14] R.D. Levine and R.B. Bernstein, *Molecular Reaction Dynamics and Chemical Reactivity* (Oxford University Press, Oxford, 1987) esp. pp. 375–376 and figure 6.60.
[15] T. Ikeshoji and B. Hafskjold, Non-equilibrium molecular dynamics calculation of heat conduction in liquid and through liquid gas interface, Mol. Phys, 81(2) (1994) 251–261.
[16] I.N. Levine, *Physical Chemistry*, 5th ed. (McGraw-Hill, Singapore, 2003).
[17] C.G. Jesudason, An energy interconversion principle applied in reaction dynamics for the determination of equilibrium standard states, J. Math. Chem. (JOMC) 39(1) (2006) 201–230.
[18] K.J. Laidler, *Chemical Kinetics*, 3rd ed. (Harper & Row, New York 1987) esp. pp. 74–75.
[19] P. Debye, *Polar Molecules*-1929 reprint edn (Dover Publications Inc, New York, 1945).
[20] C.T. O'Konski and A.J. Haltner, Characterization of the monomer and dimer of tobacco mosaic virus by transient elastic birefringence relaxation of optically anisotropic crystals, J. Am. Chem. Soc. 78 (1956) 3604–3610.
[21] S. Broersma, Rotational Diffusion constant of a cylindrical particle, J. Chem. Phys. 32(6) (1960) 1626–1631.
[22] R. Moog, D. Bankert and M. Maroncelli, Rotational diffusion of Coumarin 102 in Trifluoroethanol: the case for solvent attachment, J. Phys. Chem. 97 (1993) 1496–1501.
[23] A. Srivastava and S. Doraiswamy, Rotational diffusion of Rose Bengal, J. Chem. Phys. 103(14) (1995) 6197–6205.
[24] R.K. Pathria, *Statistical Mechanics (2le)* (Butterworth-Heinemannm, Oxford, 2001).
[25] R.M. Lynden-Bell, Comparison of the results from simulations with the predictions of models for molecular reorientation, in: A.J. Barnes, W.J. Orville Thomas and J. Yarwood eds.,

Molecular Liquids—Dynamics and Interactions (D. Reidel Publishing Co., Dordrecht/Boston/ Lancaster, 1984) pp. 501–518.

[26] D. Levesque and L. Verlet, Computer "experiments" on classical fluids, III. time dependent self-correlation functions, Phys. Rev. A 2(6) (1970) 2514–2528.

[27] K. Nakanishi, K. Toukubo and N. Watanabe, Molecular dynamics studies of Lennard-Jones liquid mixtures: further calculation on the behavior of one different particle as a model of real fluid systems, J. Chem. Phys. 68(5) (1978) 2041–2045.

[28] C.G Jesudason, *Examples Include W.C.N.A 2004* (Orlando, Florida, U.S.A, 2004) and in presentation entitled Equilibrium properties of a hysteresis dimer molecule from MD simulations using two-body potentials, in: *International Conference on Numerical Analysis and Applied Mathematics 2005*, eds. T.E. Simos, G. Psihoyios and Ch. Tsitouras (Wiley-VCH, Weinheim, 2005) pp. 287–290.